Supplement of Biogeosciences, 23, 3179–3194, 2026
https://doi.org/10.5194/bg-23-3179-2026-supplement

Biogeosciences Open Access EGU

Supplement of

Complexity in biogeochemical models: consequences for the biological carbon pump

Jonathan Rogerson et al.

Correspondence to: Jonathan Rogerson (jonathan.rogerson@lsce.ipsl.fr)

Introduction

This supplementary section provides additional details and supporting analyses related to the main manuscript. It includes the following:

S1 Regional Carbon Cycle Assessment and Processes (RECCAP2) biomes

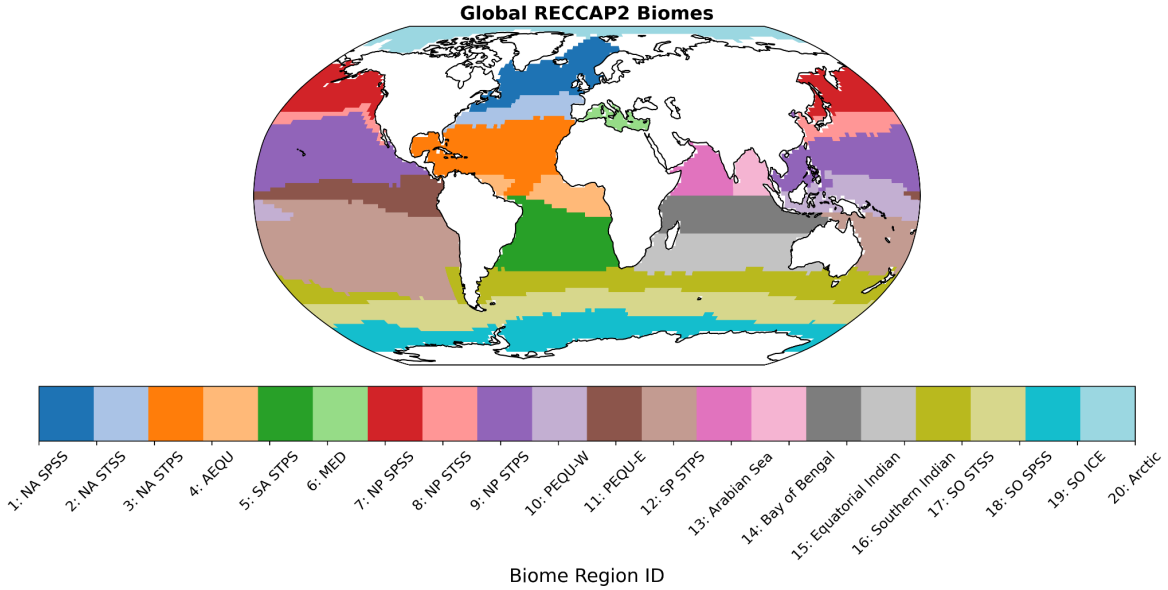

Figure S1: RECCAP2 biomes, based on Fay and McKinley (2014)

S2 Different remote-sensing NPP algorithms

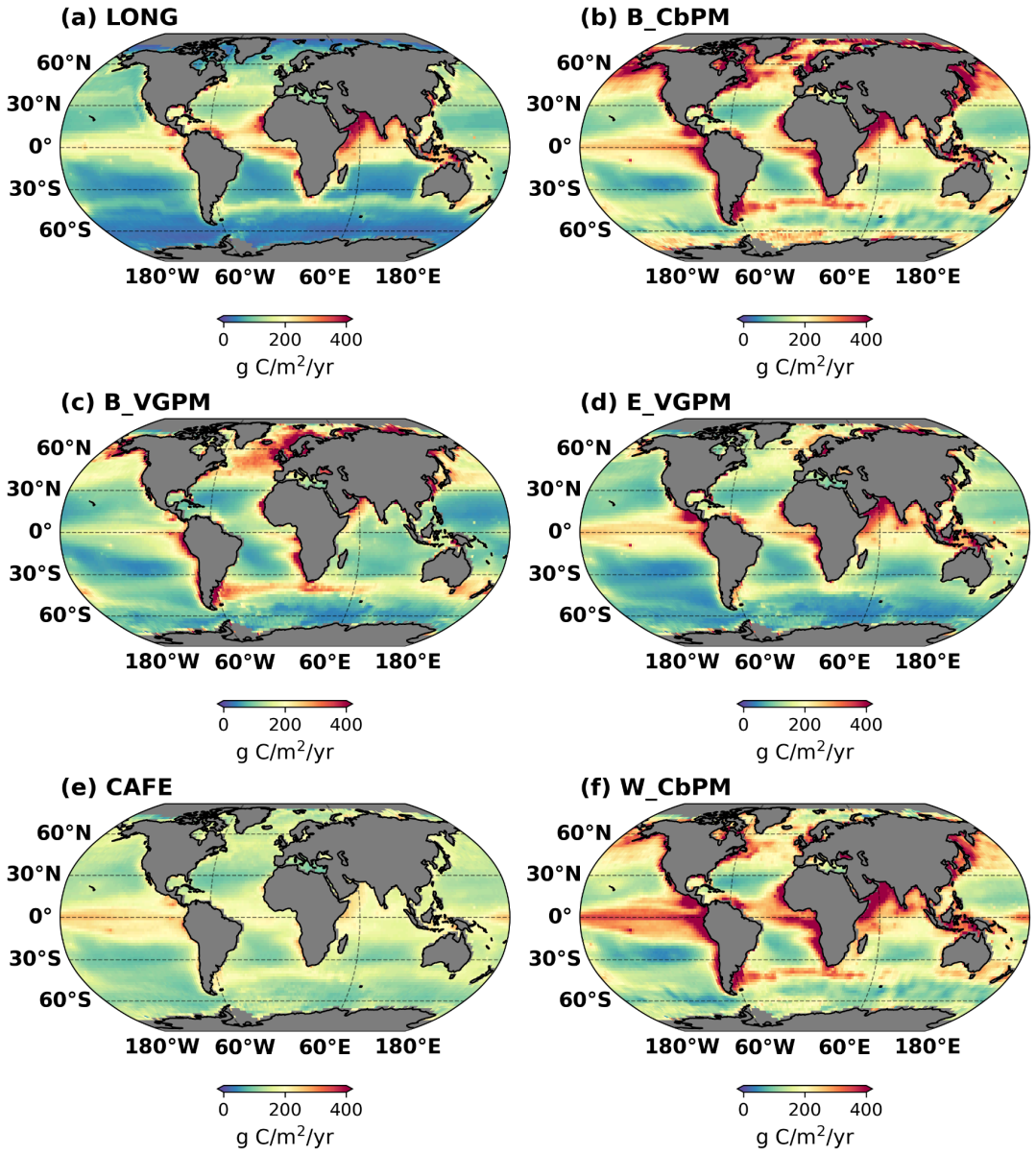

Figure S2: Mean (1998-2005) of different NPP algorithms.

S3 Different remote-sensing export production algorithms

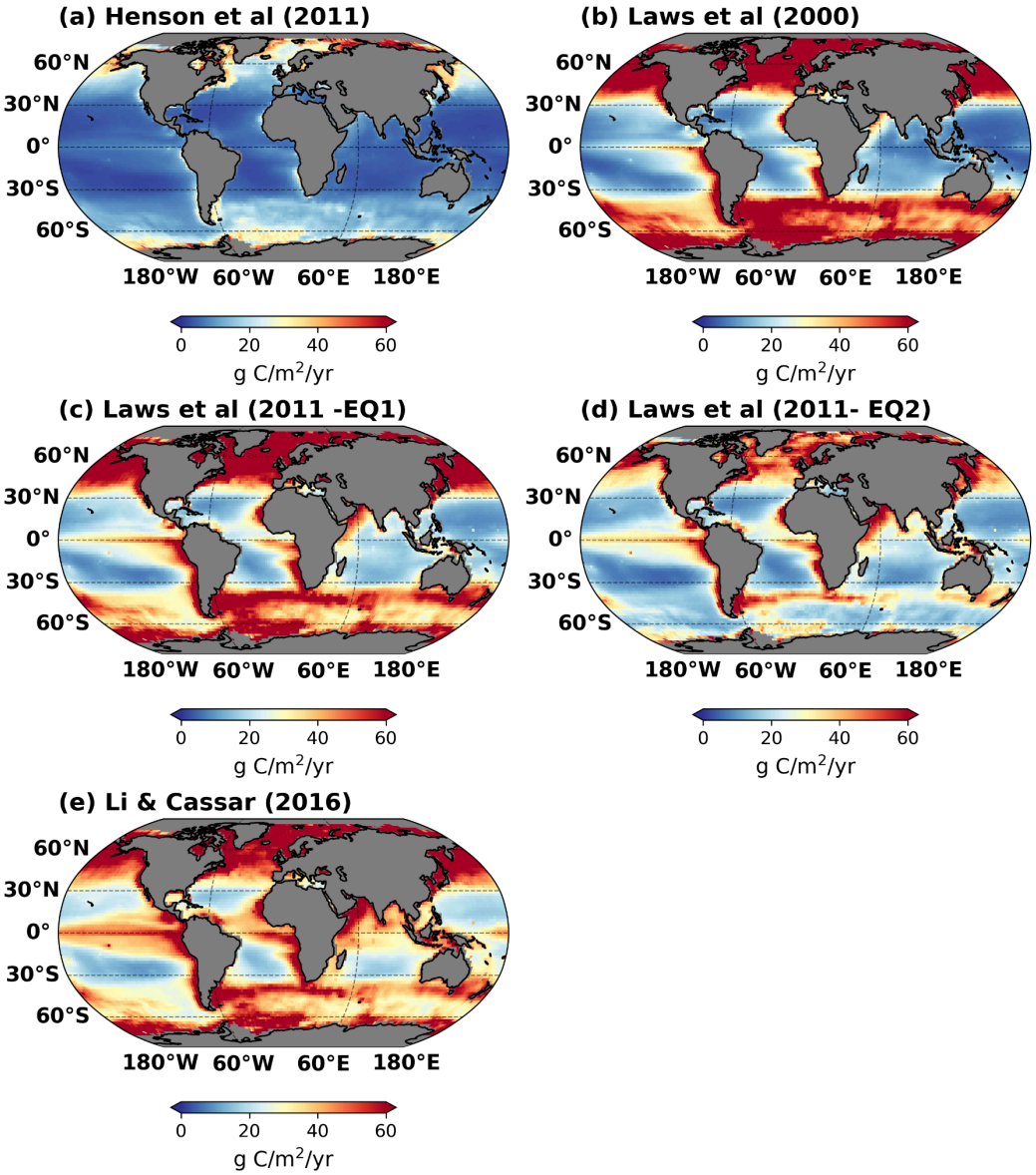

Figure S3: Mean (1998-2005) of different export production algorithms

S4 Export production equations and references

Table S1: Summary of equations used to compute export production (EP). Both NPP and EP are expressed in units of mg C m^{-2} day^{-1} and sea surface temperature (SST) in °C. The equations are written as they are shown in Jönsson et al. (2023).

Reference	Equation
Laws et al. (2000)	$EP = NPP \bullet (0.62 - 0.02\,SST)$
Henson et al. (2011)	$EP = NPP \bullet 0.23e^{-0.08\,SST}$
Laws et al. (2011) - Eq. (1)	$EP = NPP \bullet \frac{(0.5857 - 0.0165\,SST) \bullet NPP}{51.7 + NPP}$
Laws et al. (2011) - Eq. (2)	$EP = NPP \bullet 0.04756(0.78 - \frac{0.43\,SST}{30}) \bullet NPP^{0.307}$
Li and Cassar (2016)	$EP = \frac{8.57 \bullet NPP}{17.9 + SST}$

S5 Ensemble mean NPP and C_{exp} of PISCES and remote-sensing

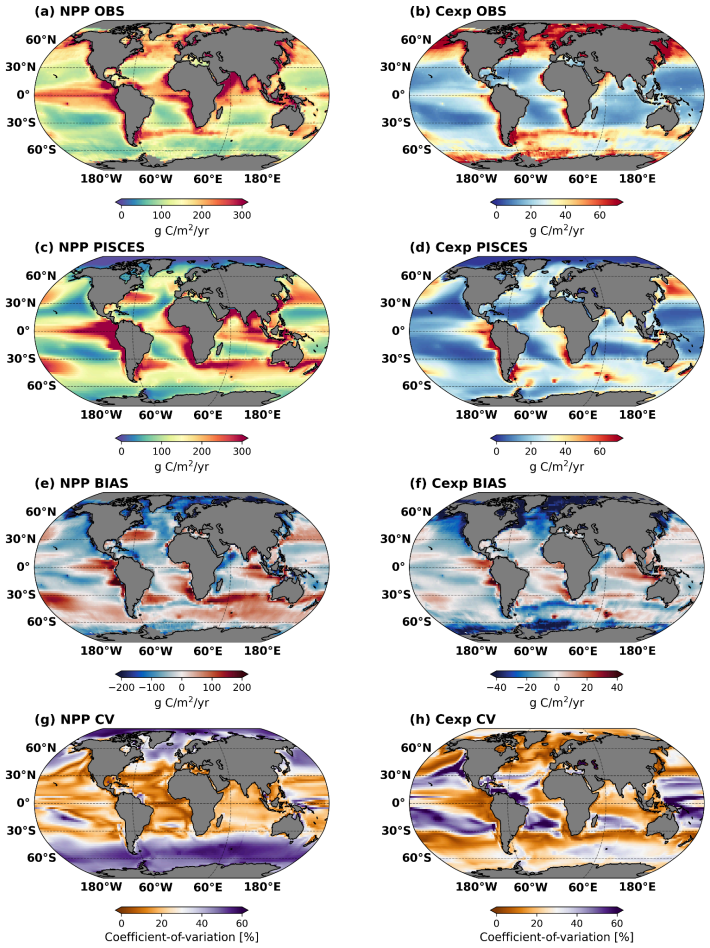

Figure S4: Global maps of satellite derived (a, b) and ensemble model mean (c, d) NPP and C_{exp}. Panels (e) and (f) show the multi-model mean minus remote-sensing bias while (g) and (h) are the coefficient of variation (CV) for model NPP and C_{exp}, respectively.

S6 N and P inventories

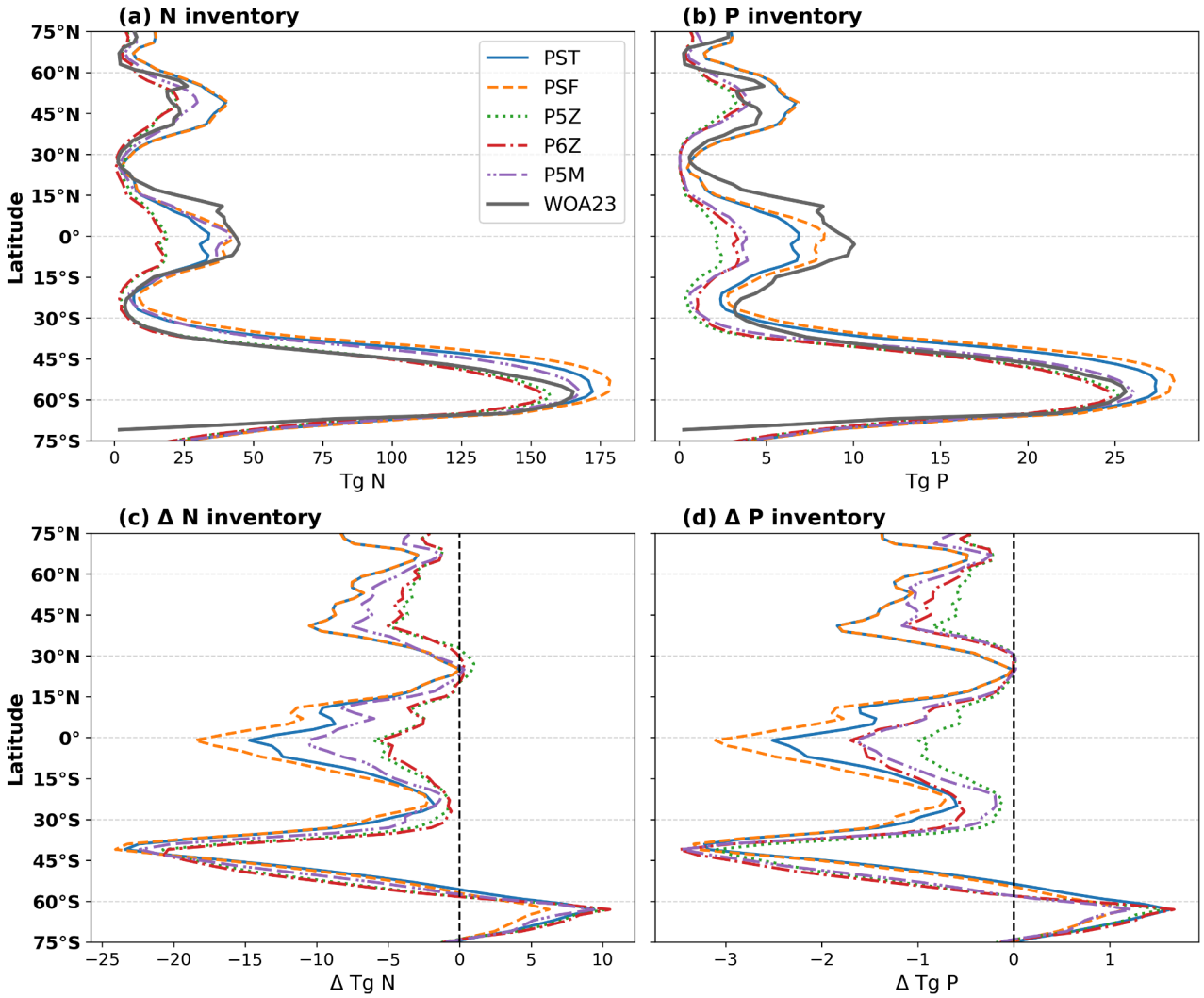

Figure S5: Zonal inventories of (a) N and (b) P integrated over the upper 100 m for the reference period. The solid black line shows data from the World Ocean Atlas 2023 (WOA23: Reagan et al., 2024). Panels (c) and (d) show future shifts in N and P, respectively.

Differences in biogeochemical parameterisations of phytoplankton growth processes across the five PISCES configurations result in some intramodel variability in N and P inventories. In Fig. (S5a, b), the Monod-quota models resolve slightly higher global nutrient inventories than the Quota-based configurations for the reference period but both modelling frameworks exhibit consistent spatial patterns; especially when compared against observational data from the WOA23. Similar future declines in nutrient inventories occur across configurations (-11.78±1.85% for N and -12.39±1.28% for P).

S7 Phytoplankton biomass percentage contribution in Quota-based configurations

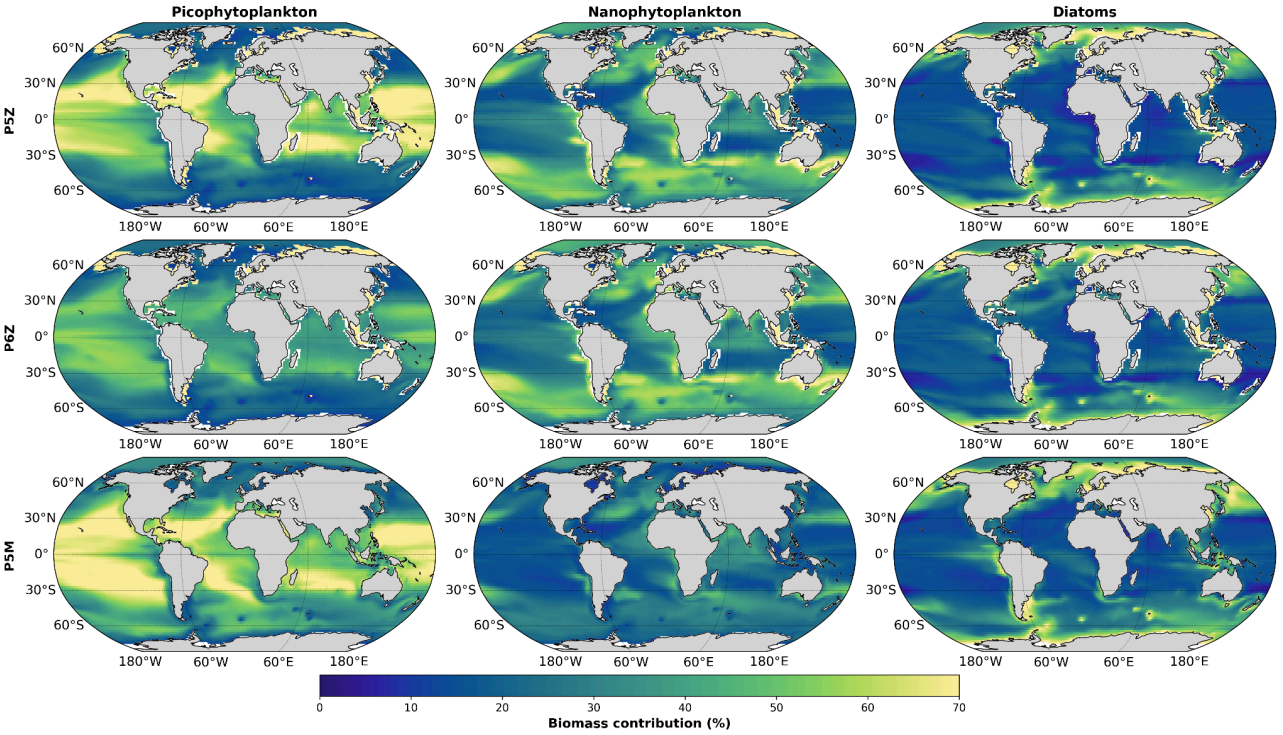

Figure S6: Percentage mass contribution of pico-, nano, and diatoms to total phytoplankton for the reference period for the three Quota-based configurations. Note that P6Z shows lower picophytoplankton biomass because part of the small phytoplankton biomass is allocated to the diazotroph PFT (not shown).

S8 Zooplankton dynamics

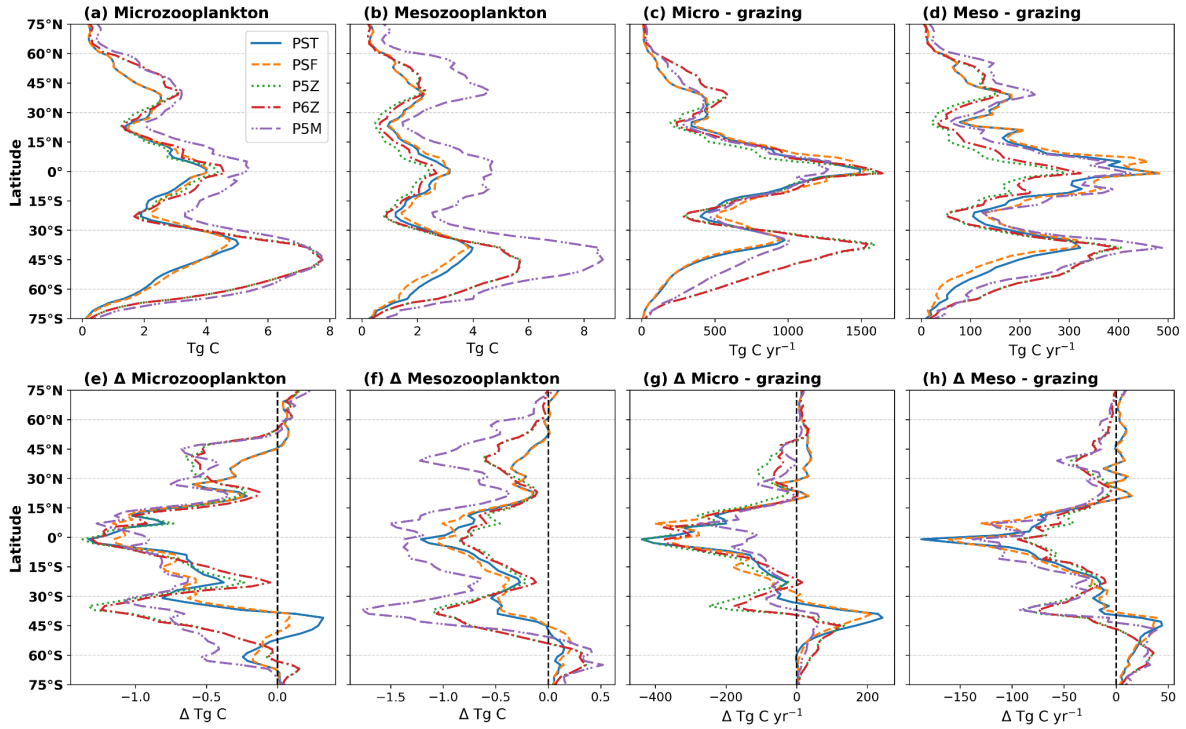

Figure S7: Top row shows zonally integrated (a) micro- and (b) mesozooplankton biomass along with the respective grazing rates over the top 100 m. Bottom row (e-h) shows the future shifts

S9 Skill assessment of PISCES configurations versus ensemble mean of remote-sensing NPP and C_{exp}.

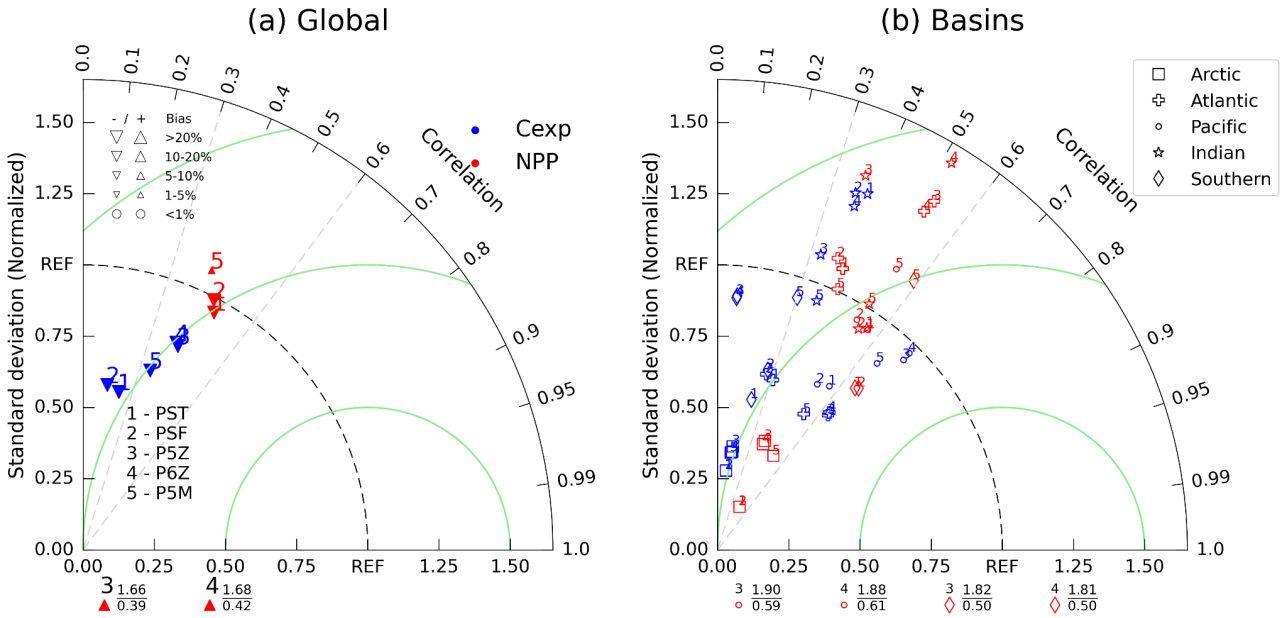

Figure S8: Taylor diagrams (Taylor, 2001) showing the (a) global and (b) basin wide performance of the PISCES configurations compared to remote-sensing. Radial distance represents the ratio of simulated to remote-sensing standard deviation and azimuthal angle is the model-data correlation. Green arcs show centered root mean square error between the model and remote-sensing estimates. In (a) and (b), numbers indicate the PISCES configuration while red and blue points correspond to NPP and C_{exp}, respectively. Outlier points are shown beneath the respective panels. Top numbers are the standard deviation and lower values are the correlation coefficient.

References

Fay, A.R., and McKinley, G.A.: Global open-ocean biomes: mean and temporal variability, Earth Syst. Sci. Data, 6(2), 273-284, https://doi.org/10.5194/essd-6-273-2014, 2014.

Jönsson, B.F., Kulk, G., and Sathyendranath, S.: Review of algorithms estimating export production from satellite derived properties, Front.Mar. Sci., 10, 1149938, https://doi.org/10.3389/fmars.2023.1149938, 2023.

Reagan, J.R., Boyer, T.P., García, H.E., Locarnini, R.A., Baranova, O.K., Bouchard, C., Cross, S. L., Mishonov, A.V., Paver, C.R., Seidov, D., Wang, Z., and Dukhovskoy, D.: World Ocean Atlas 2023, NOAA National Centers for Environmental Information [data set], https://doi.org/10.25921/va26-hv25, 2024.

Taylor, K.E.: Summarizing multiple aspects of model performance in a single diagram, J. Geophys. Res-Atmos., 106(D7), 7183-7192, https://doi.org/10.1029/2000JD900719, 2001.